Journal of Colloid and Interface Science 658 (2024) 1–11

Contents lists available at ScienceDirect

Journal of Colloid And Interface Science

journal homepage: www.elsevier.com/locate/jcis

Regular Article

Understanding the effect of moderate concentration SDS on CO_2 hydrates growth in the presence of THF

Xinrui Cai [a], Joshua Worley [b], Anh Phan [c], Matteo Salvalaglio [a], Carolyn Koh [b], Alberto Striolo [a,d,*]

[a] Thomas Young Centre and Department of Chemical Engineering, University College London, Torrington Place, London, WC1E 7JE, United Kingdom
[b] Department of Chemical and Biological Engineering, Colorado School of Mines, Golden, CO 80401, United States
[c] School of Chemistry and Chemical Engineering, Faculty of Engineering and Physical Sciences, University of Surrey, Guildford, Surrey GU2 7XH, United Kingdom
[d] School of Sustainable Chemical, Biological and Materials Engineering, University of Oklahoma, Norman, OK 73019, United States

GRAPHICAL ABSTRACT

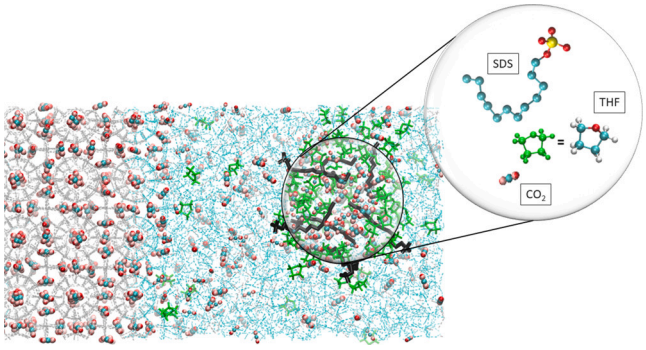

ARTICLE INFO

Keywords:
Hydrates
Promoters
CO_2
SDS
THF

ABSTRACT

Hypothesis

Additives like Tetrahydrofuran (THF) and Sodium Dodecylsulfate (SDS) improve Carbon Dioxide (CO_2) hydrates thermal stability and growth rate when used separately. It has been hypothesised that combining them could improve the kinetics of growth and the thermodynamic stability of CO_2 hydrates.

Simulations and Experiments

We exploit atomistic molecular dynamics simulations to investigate the combined impact of THF and SDS under different temperatures and concentrations. The simulation insights are verified experimentally using pendant drop tensiometry conducted at ambient pressures and high-pressure differential scanning calorimetry.

Findings

Our simulations revealed that the combination of both additives is synergistic at low temperatures but antagonistic at temperatures above 274.1 K due to the aggregation of SDS molecules induced by THF molecules. These aggregates effectively remove THF and CO_2 from the hydrate-liquid interface, thereby reducing the driving force for hydrates growth. Experiments revealed that the critical micelle concentration of SDS in water decreases by 20% upon the addition of THF. Further experiments in the presence of THF showed that only small amounts of SDS are sufficient to increase the CO_2 storage efficiency by over 40% compared to results obtained without

* Corresponding author.
E-mail address: astriolo@ou.edu (A. Striolo).

https://doi.org/10.1016/j.jcis.2023.11.136
Received 4 August 2023; Received in revised form 17 November 2023; Accepted 21 November 2023
Available online 27 November 2023

promoters. Overall, our results provide microscopic insights into the mechanisms of THF and SDS promoters on CO_2 hydrates, useful for determining the optimal conditions for hydrate growth.

1. Introduction

Clathrate hydrates are crystalline compounds. They comprise water molecules that are hydrogen-bonded to each other and guest molecules held by weak Van der Waals forces [1]. There are commonly three types of hydrate structures, namely sI, sII and sH [2]. sI is the most predominant hydrate structure on earth and contains small molecules such as CO_2 and methane [3]. Larger molecules such as Tetrahydrofuran (THF) occupy larger cages and lead to the formation of sII hydrates [4]. These compounds (sII hydrates) are commonly found under anthropogenic environments [3].

Recent studies reported that CO_2 hydrates display great potential in carbon capture [5], storage [6] and sequestration [7] due to their stability at mild operating conditions at which they can achieve relatively high gas storage [8,9]. The main obstacles for these hydrate-based technologies are slow formation rate and low thermal stability at ambient conditions [10]. For completeness, it should be pointed out that the formation of gas hydrates, when undesired and uncontrolled, can lead to negative consequences. For example, hydrates can cause flow blockage, reducing CO_2 injectivity during sequestration [11], blocking and sometimes rupturing pipelines and other equipment [12]. As these occurrences are frequently managed with the use of chemicals, it is important to understand and quantify possible synergistic and antagonistic effects among various chemicals used in the energy sector.

CO_2 hydrate formation, growth and stability can be modulated using chemical additives. These additives can be classified into thermodynamic and kinetic promoters. Thermodynamic promoters such as THF and Tetrabutylammonium Bromide (TBAB) shift the melting conditions of hydrates to milder operating conditions (higher temperature and/or lower pressure) [13,14]. On the other hand, kinetic promoters, usually surface active materials such as SDS or amino acids, accelerate hydrate growth [15–17]. Despite significant research efforts aimed at elucidating the mechanisms responsible for SDS promotion of hydrate growth, a consensus has not yet been reached. Among the numerous mechanisms proposed are the reduction of interfacial tension [18,19] and the capillary effect [20].

It has also been observed that SDS alters the surface morphology of hydrates. When SDS is present, hydrates exhibit upward growth (growth into the gas side) above the gas-liquid interface. In contrast, in systems without SDS, hydrates tend to grow downward (growth into the liquid side). These differences could affect mass transfer phenomena [21,22]. Liang et al. observed that lumps of xenon hydrates formed at low SDS concentrations, whereas a centric layer of hydrates formed at the gas-liquid interface at high concentrations [22]. They also observed that the gas uptake increases with increasing SDS concentration, but this trend ceased once the critical micelle concentration (CMC) of SDS was attained.

While promoters can enhance the formation and stability of CO_2 hydrates, they can also have negative impacts. One major drawback is that they may lead to the formation of mixed hydrates leading to lower CO_2 occupancy since the hydrate cages may be occupied by the promoters instead. For example, it has been proven experimentally that THF occupies the large cavity of sII cages hence lowering CO_2 gas uptake, especially when the THF concentration is higher than 5.56% mol [23]. However, Phan et al. [24] identified a range of temperature and pressure conditions at which CO_2 hydrates can grow in the presence of small amounts of THF, achieving fast growth rate without compromising CO_2 storage capacity. Several experiments also reported an optimal concentration for promoters, and it has been noted that adding more or fewer promoters reduces their performance [25–27].

Few studies investigated the interactions between thermodynamic and kinetic promoters on hydrate growth. For example, Torre et al. [28] reported that the combination of thermodynamic (e.g., THF) and kinetic (e.g., SDS) promoters enhances the kinetics of CO_2 hydrates better than when only a single promoter is used. Veluswamy et al. [15] also discovered that combining low concentrations of THF and SDS in an unstirred system dramatically improves the gas uptake of CO_2 in hydrates. Yet such synergistic effect only occurs under specific conditions. For instance, Wang et al. indicated that 2 mol% THF with 0.1 wt% SDS under stirring could improve hydrate formation by 12.7% as compared to the growth in a pure THF solution. However, at a higher SDS concentration of 0.2 wt%, the improvement drops to 11.7% [29]. The precise mechanism underlying these observations remains a topic of ongoing debate. Many argue that the interaction between the two additives and the interface enables the diffusion of CO_2 molecules [28,30]. Some attribute the compromised performance at high concentrations to the formation of SDS micelles [31,32].

In recent years, computer simulations have gained wide popularity as they offer a cost-effective and efficient way to predict thermodynamic and kinetic properties. By simulating the complex molecular interactions between water, CO_2 and promoters, computational simulations provide insights into the fundamental mechanisms that govern the stability and growth of the hydrates. Furthermore, computational simulations can provide a level of detail that is difficult to achieve through experimental methods alone. For instance, Phan et al. [24] recently proved, using the direct coexistence method, that THF shifts the equilibrium curve of CO_2 hydrates and facilitates CO_2 diffusivity into hydrate cages [24]. Several groups also used Monte Carlo simulations to investigate the growth of gas hydrates [33,34]. These simulation studies achieved remarkable agreement with experiments while elucidating molecular phenomena that were previously only hypothesised.

Within this landscape, we utilised atomistic MD simulations to understand hydrate growth in the presence of promoters at the molecular level. By simulating CO_2 hydrates at different temperatures and promoter concentrations, we aim to decipher the microscopic mechanism that allows THF and SDS to promote or inhibit hydrate growth. The remainder of the manuscript is organised as follows: we first introduce the simulation methodology and report a few details concerning the experimental techniques used to validate our predictions. We then discuss our results, starting from the computing simulations and continuing with the experimental validation ones. We conclude by generalising our results within the context of hydrates application in CO_2 capture, transport, and storage.

2. Methodology

2.1. Methodology

2.1.1. Simulation setup

The initial configuration of the simulation box is set up as shown in Fig. 1, where the hydrate phase is sandwiched by the bulk liquid phase along the z-direction. The hydrate slab, 4.812 nm × 4.812 nm × 4.812 nm in three dimensions, is constructed using sI CO_2 hydrate cages as it is the most stable structure under our simulation conditions [35]. The structure of the hydrate cages was built based on the work of Takeuchi [36]. In addition to the 6948 water molecules, 240 CO_2 molecules, 8 SDS molecules and different amounts of THF (0/50/100) molecules were inserted into the bulk liquid phase. The concentration of THF in the bulk would thus range from 0 mol% to 1.37 mol%, which is expected to stabilise hydrates growth [37]. Periodic boundary condi-

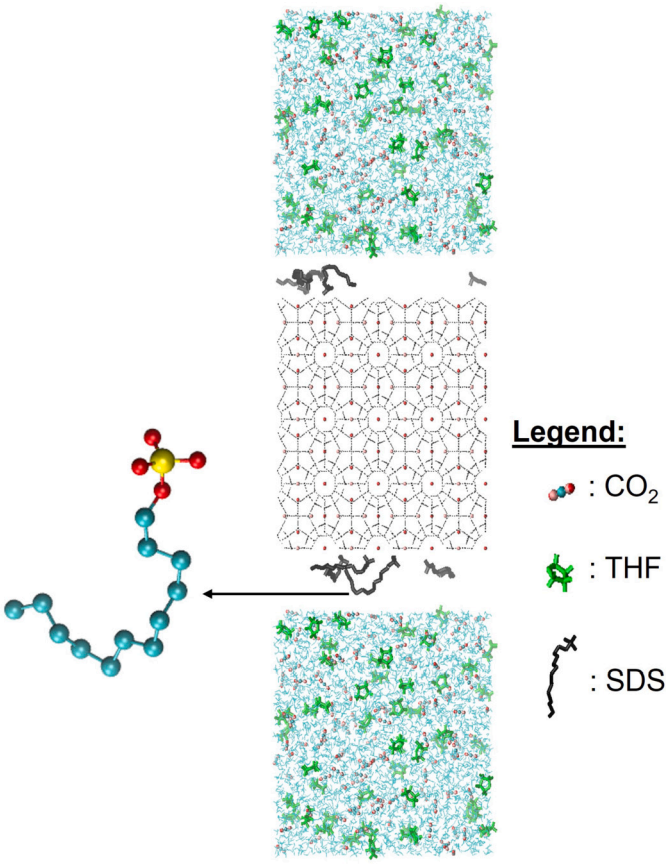

Fig. 1. Snapshot of one representative initial configuration used for molecular simulations. The cyan and grey lines represent water from the hydrate and liquid phases, respectively. Black molecules are SDS, green molecules are THF and cyan and red spheres are carbon and oxygen atoms, respectively, that together form CO_2. The chemical structure of SDS is shown on the left, where the cyan, red and yellow spheres represent Carbon, Oxygen and Sulfur atoms, respectively. (For interpretation of the colours in the figure(s), the reader is referred to the web version of this article.)

tions are applied in all directions. This renders the hydrate slab infinite in the xy direction, presenting two flat interfaces to the liquid phase perpendicular to the z-direction.

2.1.2. Molecular models and force fields

We used the TIP4P/Ice model to describe water molecules as it has been shown that this water model reproduces results that are within a variation of 5K with experimental values [38,39]. Conde et al. compared the three-phase coexistence curve for methane hydrates using TIP4P, TIP4P/2005 and TIP4P/Ice water model [40]. The coexistence temperature obtained using TIP4P/Ice agrees best with experimental results, with only a 5K difference. Miguez et al. also compared the three-phase coexistence of CO_2 hydrates. TIP4P/Ice predicts a melting point only 2K away from the experiment value [39]. The EPM2 [41] force field was used to model CO_2 molecules as several studies have shown its capability to predict CO_2 hydrates growth and dissociation [42,39]. The general AMBER force field [43] was used for modelling THF due to its prior success in THF hydrate simulations [24]. SDS molecules were modelled by implementing the TraPPE force field for the hydrocarbon tail [39] and the Berkowitz model for the headgroup [44]. Non-bonded interactions are modelled using electrostatic and dispersion forces. We used Coulomb interaction for electrostatic forces with a cut-off at 1.4 nm, and the particle mesh Ewald method was chosen for long-range corrections. Lennard-Jones interactions were used for modelling the dispersion forces with a cut-off of 1.4 nm. Lorentz-Berthelot combining rules were used to estimate the LJ interactions between dissimilar atoms.

Numerous studies have substantiated the reliability of these forcefields [39,40,42]. For instance, Phan et al. [24] utilised TIP4P/ice, EPM2 and general AMBER forcefields to simulate CO_2 hydrates. Using these forcefields, the hydrates grow at 269.1 K and 274.1 K but initiate dissociation at a temperature of 279.1 K. This dissociation temperature conforms to experimental observations.

2.1.3. Algorithm

We employed the direct coexistence method to simulate the growth and dissociation of CO_2 hydrates where the solid hydrate phase is in direct contact with the bulk liquid phase [45]. We describe the systems with atomistic resolution and integrate the equations of motion using the software package GROMACS 2021 [46]. The leapfrog algorithm is used to solve the equation of motion with a 1 fs timestep. Once the initial configuration is prepared (see Fig. 1), our protocol initiates with an energy minimisation via the steepest descent method. The system is simulated under NPT constraints for 5 ns to equilibrate the pressure utilising Berendsen's pressure coupling [47] with a time constant of 5 ps. The temperature is controlled using the Nosé-Hoover thermostat with a time constant of 0.5 ps [48]. As shown in Supplementary Information (Figure S2), analysis of the simulation results confirms that both the pressure and the volume of the simulation box converged during the equilibration phase of our simulations. Finally, 600 ns NPT simulations were performed using Nosé-Hoover thermostat and Parrinello-Rahman barostat [49] to produce the results presented. The temperature and pressure were coupled at a time step of 0.5 ps. This ensures the rapid removal of latent heat released to the system by the phase transition [50]. By using a semi-isotropic pressure coupling while maintaining the xy interfacial area constant, the system maintained the pressure normal (z direction) to the hydrate-liquid interface constant. This approach is commonly implemented to avoid anisotropic pressure distributions due to the fact that the hydrate substrate is solid, hence its dimensions cannot be changed to maintain the desired constant pressure [51]. The melting temperature of CO_2 hydrates at a pressure of 25.5 bar is experimentally determined to be 279.1 K [52]. Our system is simulated at 269.1 K, 274.1 K, 279.1 K and 284.1 K and a pressure of 25.5 bar. We extracted the configuration at every 50 ns interval as the input and simulated it for a production phase of 1 ns used for analysis. The average box size during the simulation run was found to be 4.812 nm, 4.812 nm, 14.83 ± 0.15 nm in the x, y and z directions, respectively.

2.1.4. Thickness analysis

The growth and dissociation of the hydrate slab are calculated by quantifying its thickness as a function of simulation time. Whether water molecules are organised within the crystalline hydrate or are instead disordered in a liquid film is determined by quantifying the F4 order parameter using equation (1) [53] applied every 50 ns of simulations

$$F4 = \frac{1}{k}\sum_{1}^{k} cos3\phi \tag{1}$$

In equation (1), ϕ refers to the H-O ... O-H torsional angle and k refer to the number of H-O...O-H bond pairs with bond length < 0.35 nm. The F4 value for water molecules embedded in a hydrate environment is approximately 0.7, while that for water molecules in the liquid phase is close to 0 [54,55]. This difference allows us to discriminate between hydrate and liquid phases, as illustrated in Figure S5 in supporting materials. The region between the bulk liquid and hydrate is the interfacial transition region, where partial hydrate cages are formed. The hydrate thickness is attained by measuring the width of the region when F4 > 0.3. The F4 value is computed from 1 ns simulations initiated from structures extracted at 50 ns intervals. Each of the 1 ns simulations is repeated 5 times by running MD simulations in series with the same initial configuration to attain an error bar associated with hydrate thickness.

Table 1
Heat of formation and hydration number for CO_2 and CO_2-THF hydrate.

-	Heat of Formation (kJ/mol)	Hydration Number	Reference
CO_2 Hydrate	70.8	5.9	[37,59]
CO_2-10wt% THF	126.2[1]	20	[37,60]

[1] There is a wide spread in heat of formation predictions for THF-CO_2 hydrates. This value was selected as it was calculated at nearly identical conditions to the present studies.

In the Supporting Information (Figure S4) we provide a representative set of simulation results in which prominent changes in system size appear to have minimal impact on the growth or dissociation of hydrates.

2.1.5. Clustering analysis

An algorithm was implemented using PLUMED to identify and analyse the largest cluster of SDS molecules in solution. To this aim, we exploit the contact matrix to define a graph of connected SDS molecules and then determine the largest SDS cluster corresponding to the largest connected component of the graph [56,57]. This is done by computing the distance between the centre of mass of each SDS molecule and defining them as bonded when the distance between their centres of mass is <0.8 nm. Once the molecules belonging to the largest cluster are identified, we compute the centre of mass of the cluster and its diameter. CO_2 and THF molecules are considered trapped in the SDS cluster when found within the identified cluster radius. This procedure allows us to obtain aggregate size, aggregation number, and composition within an aggregate as the simulations progress.

2.1.6. Experimental - pendant drop tensiometry

An ambient condition pendant drop tensiometer (KSV instruments) was utilised to determine the CMC of SDS and SDS-THF solutions. A sketch of the experimental set-up is presented in Figure S6. CO_2 saturated de-ionised (DI) water was first prepared by bubbling CO_2 through a beaker of DI water for 12 hours. SDS solutions were then prepared from 0.001M to 0.015M by dissolving SDS into the CO_2 saturated water. These solutions were allowed 24 hours to reach equilibrium. The entire series was tested via the pendant drop technique with the drop suspended in an open cuvette and monitored for 5 mins for each concentration tested. A total of 3 drops were tested for each concentration to produce an average surface tension value. The surface tension (ST) of each solution was calculated by solving the Young-Laplace equations for each droplet and plotted against the log of concentration to determine the switchover from the concentration-dependent ST region to the concentration-independent region. A similar methodology was used to obtain the ST of SDS in a SDS-THF-CO_2 solution. 0.476M of THF was added to SDS solutions ranging from 0.001M to 0.038M SDS, and ST was tested after a 5 min equilibration period which would minimise THF evaporation but still allow equilibrium to be reached.

2.1.7. Experimental - high-pressure differential scanning calorimetry (HP-DSC)

A high pressure - low temperature Differential Scanning Calorimetry (HP-DSC) apparatus (Setaram microDSC VIIa) was utilised for hydrate growth testing. The experimental setup is illustrated in Figure S7. Pure CO_2 hydrates and CO_2 hydrates formed with a combination of THF and SDS were examined to determine the effect of the combination of promoters on hydrate growth and CO_2 uptake.

For the pure CO_2 hydrate experiments, approximately 15 mg of DI water was added to the DSC cell, which was then sealed and placed into the apparatus. The cell was pressurized to 25.5 bar using CO_2 gas (99.998%, General Air). The sample was cooled to 253.15 K and then heated to 293.15 K at a rate of 1 K/min for the first cycle to form ice and hydrate and induce the memory effect, then three repeat experiments were performed with the same limits and a cooling rate of 0.2 K/min to measure the heat released during dissociation.

For the CO_2-SDS tests, the same procedure was followed except that 0.001M and 0.038M solutions of SDS (>99.0%, Sigma Aldrich) in DI water were loaded into the cell. For the tests that involved the usage of THF, 10wt% solutions of THF (>99.9%, Sigma Aldrich) and DI water were loaded into the cell along with different concentrations of SDS solutions if needed. In these THF-related tests, the lower temperature limit was increased to 263.15 K to maintain the same subcooling as for the CO_2 and CO_2-SDS tests. All other parameters were the same. Conversions for CO_2 containing hydrates from each test were calculated in the same manner as [58] utilising the constants in Table 1.

For the conversion calculations, all hydrates containing THF and CO_2 were assumed to have a heat of dissociation similar to the 10wt% THF system. In cases where multiple peaks were discerned, the peaks were first identified and separated by the onset temperature and peak maximum temperature to determine which phase was likely present (CO_2 or CO_2-THF hydrate). The heat of dissociation corresponding to that phase was utilised for the estimates provided herein. Subsequently, the conversion was computed for each isolated peak, and the resulting values were summed up to determine the overall total conversion.

3. Results and discussions

3.1. Simulated hydrate growth/dissociation

Fig. 2 presents the simulation results obtained for the hydrate growth profiles at all temperatures and THF concentrations considered. The trend line for the growth profile is computed using logistic regression via Python's sklearn linear regression library. As seen in Fig. 2, the hydrates grow or dissociate quickly within the initial 100 ns and their thickness reaches a plateau after that. This is due to the change in the composition of CO_2 in the bulk liquid, which alters the concentration driving force for hydrates growth/dissociation.

From the analysis of the growth profile, we observed that hydrates grow when $T < 279.1$ K. The melting temperature for systems without a thermodynamic promoter (THF) can be inferred as 279.1 K, as the hydrate thickness stays roughly constant during our simulations at this temperature. This agrees well with experimental results where the melting temperature is determined to be around 279.1 K [52]. For the systems with THF present at $T = 279.1$ K, there is a minor growth at the beginning, but the thickness soon reaches a plateau. The plateau could be due to the reduction in driving force as CO_2 hydrates are formed or to the formation of micelle-like aggregates that will be discussed in section 3.3. Above 279.1 K, our results show signs of hydrate dissociation, which conforms with experiments [61,52]. Noticeably, the logistic regression fits the growth profile well at low temperatures. As temperature increases beyond 279.1 K, the hydrate growth becomes unstable, and the logistic regression model underfits the simulation data, especially when no THF is present. This behaviour is expected, as experiments have shown that the hydrate structure fluctuates between dissociation and formation at moderately high temperatures [62]. In this study, we focus on hydrate growth at low temperatures, where logistic regression is effective in describing hydrate growth. We next discuss the results obtained in the presence of SDS.

3.2. Aggregate formation

Visual analysis of the simulation trajectories reveals that SDS molecules aggregate at high temperatures ($T \geq 274.1$ K). To further analyse the aggregation content, we plot the component concentration profiles at the end of each simulation, i.e. at 600 ns.

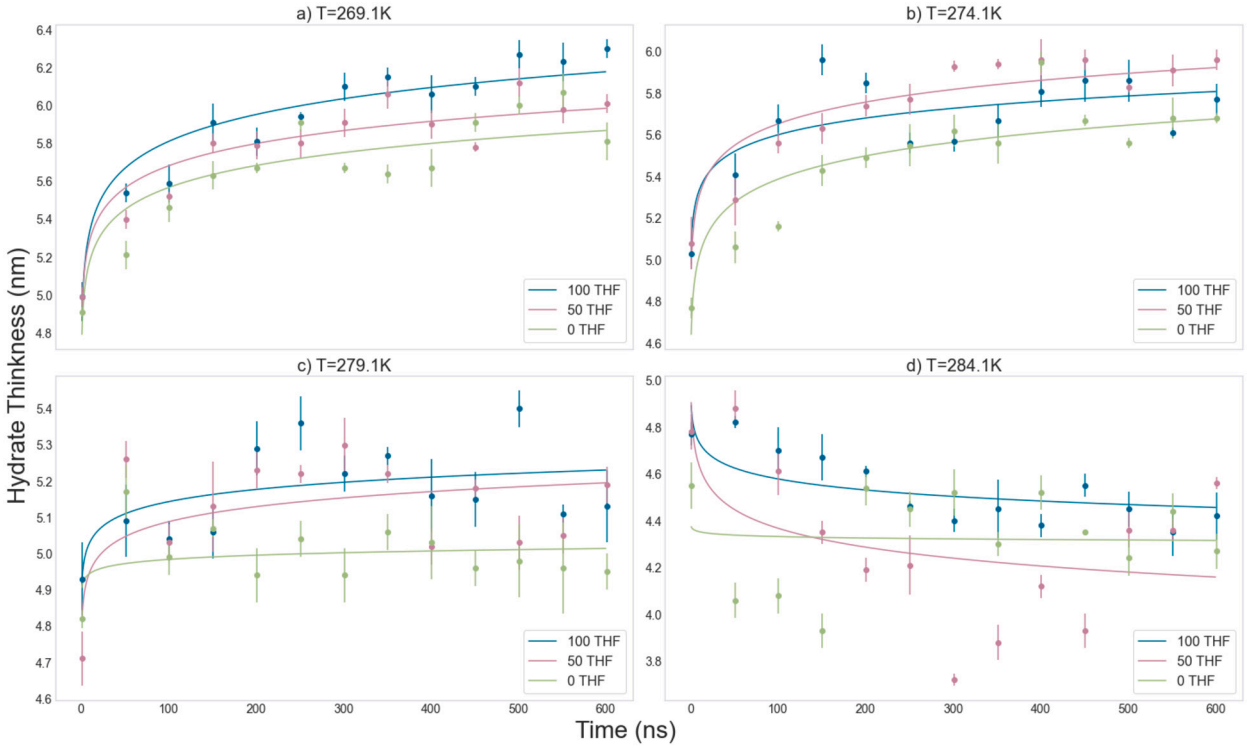

Fig. 2. Comparison of hydrate thickness evolution over time with 0/50/100 THF molecules in the system at a) T = 269.1 K, b) T = 274.1 K, c) T = 279.1 K and d) T = 284.1 K. The error bars at 0 ns represent the variations of hydrate thickness from 0 ns to 1 ns.

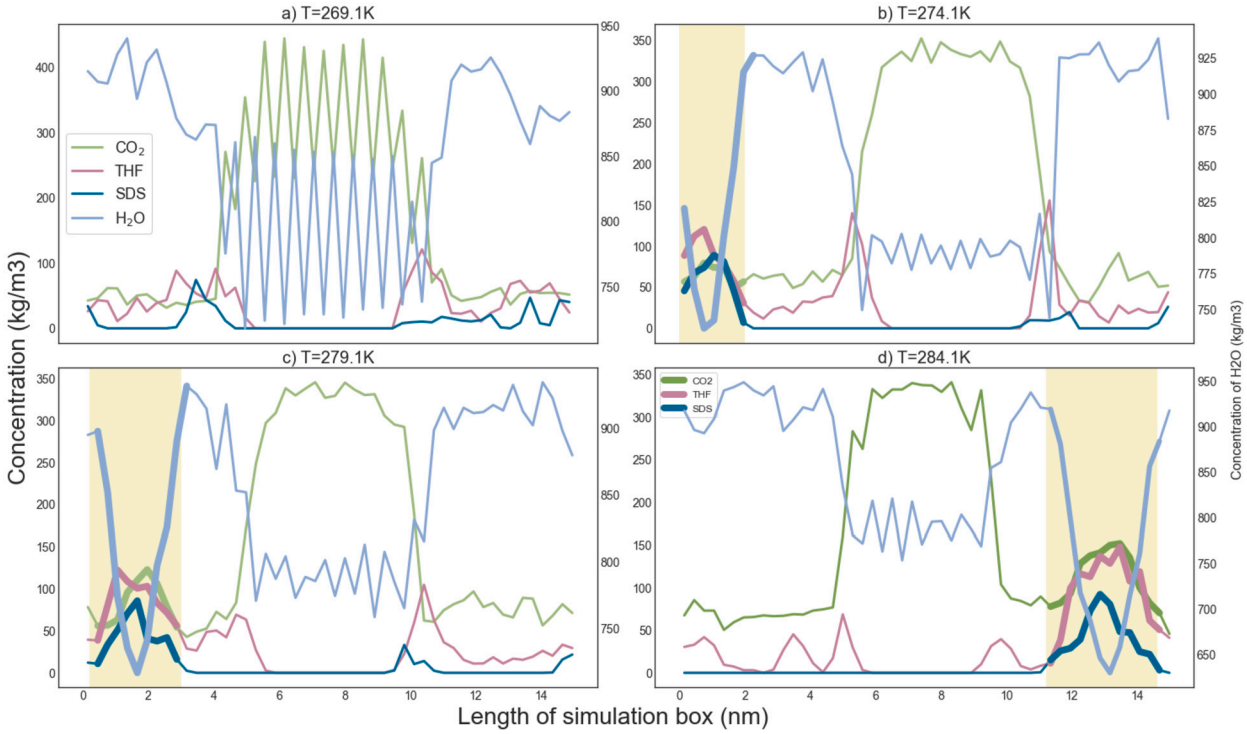

Fig. 3. Concentration profiles of CO_2, THF and SDS molecules within the simulation box with 100 THF molecules at a) T = 269.1 K, b) T = 274.1 K, c) T = 279.1 K, d)T = 284.1 K. The highlighted regions indicate the position of the aggregate containing SDS, THF and CO_2.

There is no discernible concentration peak at T = 269.1 K as illustrated in Fig. 3 (a), which reinforced the observation that no aggregation occurred at this temperature. The lines from Fig. 3 (b) are translated to the right along the x-axis by 0.25 nm for a clearer identification of the aggregation cluster. In Fig. 3 (b), (c) and (d), the SDS concentration peaks shown in the bulk liquid phase indicate the position of the aggregates. The alignment of THF and CO_2 concentration peaks with those of SDS indicates that the aggregates also contain CO_2 and THF molecules. This is confirmed by visual analysis of the simulation snapshots. There is also a significant reduction of H_2O within the ag-

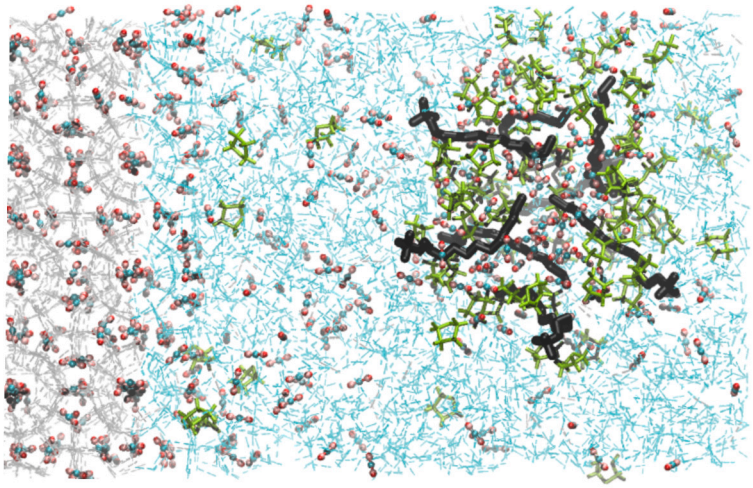

Fig. 4. Snapshot of SDS aggregates at T = 284.1 K where the black molecules are SDS molecules.

Table 2
Summary of SDS aggregates formation under different temperatures and THF concentrations. In this table, 'micelle' stands for surfactant aggregate.

Temperature	0 THF	50 THF	100 THF
269.1 K	No micelle	No micelle	No micelle
274.1 K	No micelle	No micelle	Micelle
279.1 K	No micelle	Micelle	Micelle
284.1 K	No micelle	Micelle	Micelle

gregates, which indicates that a hydrophobic environment would have formed. A closer look at the simulation snapshots using the software VMD (Fig. 4) confirmed that the SDS hydrophobic tails always point towards the centre of the aggregates. In contrast, the hydrophilic head groups face towards the aqueous phase. Such characteristics suggest that the SDS molecules within the system have formed a micelle-like structure.

The aggregates observed in our simulations appear to be roughly spherical in shape, which is typical of an SDS micelle in water at low concentrations [63]. However, SDS micelles in water at ambient conditions are usually between 3.5 to 4 nm in size, much larger than the aggregates obtained within our system, whose size is approximately 2.5 nm. Additional simulations have been performed, from which it can be seen (Figure S3) that a bigger simulation box would result in a larger SDS aggregate, but the increase is minimal. Such minor differences also have insignificant impact on the overall thickness of the hydrate as seen in Figure S4.

To understand why SDS molecules in the simulated system yield aggregates at conditions where micelles are not expected in bulk liquid water, we conducted a systematic study in which temperature and composition were changed.

As seen in Table 2, we did not observe aggregation in the systems with no THF, even at the highest temperature considered. The aggregate phase transition temperature increased when the number of THF molecules added to the system was halved. Such observation implies that THF reduces the CMC of SDS. The potential reason for this phenomenon is that THF may become more insoluble as temperature increases due to the closed-loop miscibility gap within the THF-water binary system [64]. Should this be the case, then the insolubility of THF in water at the simulation temperature creates an entropic driving force that induces the formation of micelle-like aggregates [65]. Prior studies also established that the CMC of SDS surfactants decreases linearly with a higher concentration of ethers [66], further reinforcing our hypothesis.

Figure S8 shows the number of THF molecules trapped within the SDS aggregates over the entire trajectory at 274.1 K (smallest aggregate) and 284.1 K (largest aggregate). The results are obtained using the clustering algorithm described in the Methods section. The number of molecules adsorbed increases initially and reaches a constant value when the aggregate is saturated, which is in line with typical micellar behaviour. Noticeably, the aggregates trapped more THF molecules at higher temperatures.

At the pressure and concentration conditions used in our set-up, THF will become insoluble between T = 368 K to 404 K [67], which is warmer than the temperature within our system. However, the miscibility behaviour of THF in water is highly sensitive to contamination, and therefore the presence of CO_2 and SDS may alter the miscibility curve [64].

3.3. Aggregates effects on hydrates growth

The effect of the SDS aggregates on the growth of hydrates can be deduced from Fig. 2. At T = 269.1 K (Fig. 2(a)), where no SDS aggregate is formed in any of the three systems, the hydrates have a higher growth rate with increasing THF concentration. Similar phenomena are also observed at T = 279.1 K (Fig. 2(c)), where systems with THF form SDS aggregates and agree well with previous studies by Phan et al. [24]. However, at T = 274.1 K, the aggregate is formed only in the system with 100 THF. The hydrate growth profile in this system (Fig. 2(b)) shows a slower hydrate growth rate than the system without SDS aggregate, despite having more THF. This implies that the SDS micellar aggregate impedes hydrate growth.

Though SDS is generally regarded as a kinetic promoter for gas hydrates, several studies reported that increasing SDS concentration beyond certain limit compromises hydrates growth [25,32]. Experiments showed that the promotion effect of SDS drops beyond its CMC [31]. Although our observations are obtained at very low SDS concentrations (0.11 mol%), it should be pointed out that the simulated SDS molecules are initially placed near the hydrate-liquid interface (Fig. 1). This is because the time scale accessible to atomistic MD simulations is on the order of hundreds of nanoseconds, while the typical exchange rate between surfactants in the bulk and those adsorbed at interfaces or within micelles is of the order of microseconds. Nevertheless, the simulation and the experimental results just summarised are in qualitative good agreement.

To identify the molecular mechanism responsible for the observations, we hypothesise a kinetic or thermodynamic effect. In the next paragraphs, we discriminate between the two possibilities.

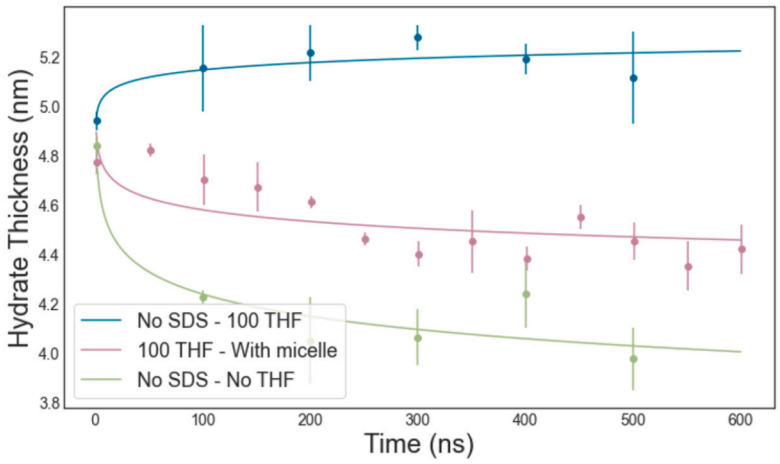

Fig. 5. Comparison of hydrate growth removing SDS and CO_2 within SDS aggregates with literature value with no SDS at T = 284.1 K [24].

3.3.1. Hypothesis 1: kinetic effects

Lv et al. [32] identified an optimal concentration of surfactant promoters concerning the growth of methane hydrates. Adding promoters beyond the optimal amount leads to a decrease in hydrate growth rate and gas storage capacity. They hypothesised that such phenomena can be ascribed to micelles forming cages that will trap the gas molecules, hindering mass transfer from the liquid to the hydrate. Stimulated by this hypothesis, we delved further into understanding micelles' kinetic and thermodynamic influences on hydrate growth.

If the SDS aggregates reduce the kinetics of hydrate growth by removing CO_2 from the system, it is plausible that the aggregation would lead to a decrease in the concentration of CO_2 at the interface, which is the rate-limiting step for hydrate growth [68]. Since we observe the presence of SDS aggregates in our systems alongside CO_2, it is reasonable to assume that these aggregates have an impact on the concentration of CO_2 at the interface. Hence, the concentration of CO_2 at the hydrate-liquid interface is analysed at T = 284.1 K, at which conditions our simulations identify the largest SDS aggregate. The results are illustrated in Figure S9. We acquired interfacial concentrations by identifying the interface using the F4 order parameter and calculated the concentration within the interfacial region (≈1 nm thick). It can be inferred from the graph that there are somewhat fewer CO_2 molecules at the interface when the SDS aggregate is present (when THF is present), which agrees with the mass transfer limitation hypothesis by Lv and colleagues [32]. However, statistical analysis reveals a different conclusion. We conducted a two-sided t-test between the 100 THF system (which has the largest SDS aggregate) and the 0 THF system using Python's scipy library. The p-value obtained is 0.076, which is slightly higher than 0.05, suggesting that the difference in CO_2 concentration at the interface is not statistically significant. As such, though it is possible that mass transfer limitation could be a factor in the observed behaviour, this hypothesis cannot be conclusively verified.

3.3.2. Hypothesis 2: thermodynamic effects

Because the aggregates adsorb and trap a significant amount of THF and CO_2 molecules, impacts could be exerted on hydrate growth. First, trapping the THF molecules will reduce their promoting capability. Second, trapping CO_2 will reduce supersaturation and hence the driving force for hydrate growth.

Fig. 5 demonstrates the difference in hydrate growth between our systems and the results reported by Phan et al. [24]. Their work employed an identical simulation framework to the one considered here, except no SDS was present. In other words, no aggregate formed in the systems studied by Phan et al. We obtained the hydrate thickness data from two of their systems: one with 100 THF and one without at T = 284.1 K. Our THF and CO_2 concentration and simulation conditions are also identical. Their results indicated that THF shifts the equilibrium curve to milder conditions, as the hydrates with THF promoters (blue) did not dissociate as much as those with no THF (green). Our system with 100 THF and SDS at T = 284.1 K lies in between the other two datasets. It is, therefore, apparent that the SDS molecules behave like thermodynamic inhibitors. Figure S8 shows that approximately 50 to 60 THF molecules are trapped within the SDS aggregate. As such, Fig. 5 can be viewed as the hydrate growth comparison between systems with 100 THF, 50 THF and 0 THF. The trend illustrated in Fig. 5 agrees well with our simulation results at T = 269.1 K and T = 279.1 K, where more THF leads to faster growth, as shown in Fig. 2. This observation supports the hypothesis that SDS aggregate traps THF molecules, removing them from the hydrate-liquid interface. This mechanism could only partially explain the slower hydrate growth rate obtained for the system with 100 THF compared to 50 THF at T = 274.1 K, as illustrated in Fig. 2 (b). The SDS aggregate in the 100 THF system only traps 20-30 THF molecules, which means there are still more free THF in this system than in the one built to contain 50 THF molecules. This leads us to the second thermodynamic hypothesis: that the aggregates reduce the driving force by sequestering CO_2 molecules.

To test this possibility, we conducted additional simulations to understand the significance of reduced CO_2 concentration in the bulk liquid on hydrate growth. We used the same conditions and configurations as the 100 THF system at T = 274.1 K, but we removed the CO_2 and THF content trapped in the aggregate. To prevent SDS from aggregating, we reduced the hydrocarbon tail to only 5 carbon chains so as to increase its CMC. Though this would cause a slight deviation in chemical properties from SDS, the change in tail length has a limited impact on hydrate growth at a concentration above 0.1wt% [69], which is significantly lower than the concentration of SDS used in our simulations. The growth profile obtained is presented in Fig. 6. It can be deduced from the graph that reducing CO_2 concentration slows down hydrate growth. However, the data sets are within statistical uncertainty from each other, suggesting that reducing CO_2 concentration is not the only mechanism by which the aggregates affect hydrates growth.

4. Experimental validation

The simulation studies discussed above reveal two significant observations. Firstly, it is observed that THF decreases the CMC of SDS. Secondly, the occurrence of SDS aggregates adversely affects the growth of hydrates. These conclusions were validated using experiments.

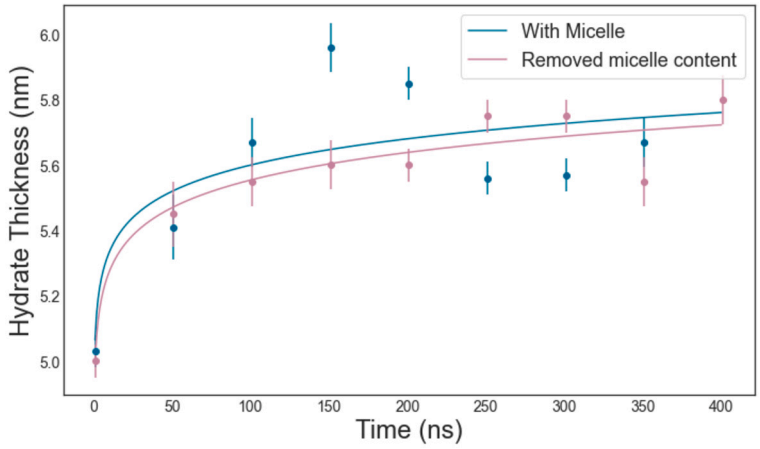

Fig. 6. Comparison of hydrate growth removing SDS and CO_2 within SDS aggregates with literature results in the presence of no SDS at T = 284.1 K.

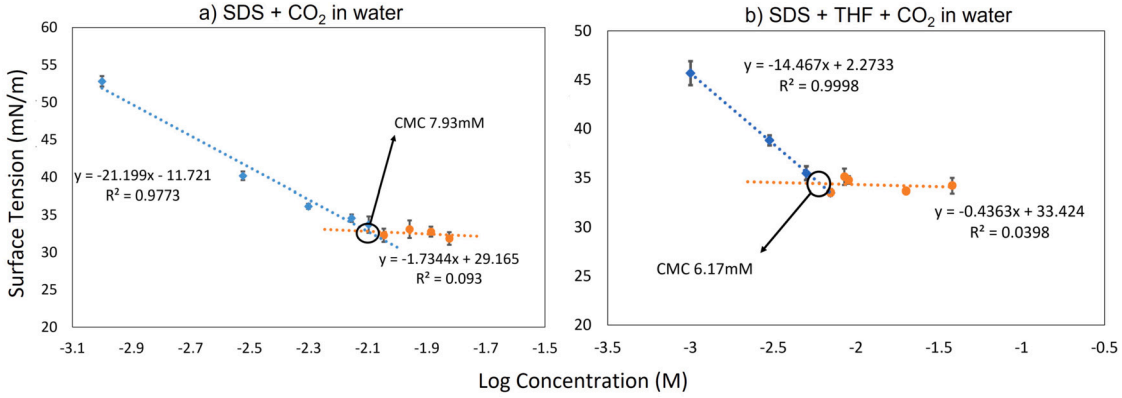

Fig. 7. Surface tension vs log concentration for a) pure SDS solutions in CO_2 saturated water from 0.001M to 0.015M SDS with CMC determined as 7.93mM SDS, and b) THF-SDS solutions in CO_2 saturated water from 0.001M to 0.038M SDS with 0.476M THF with CMC determined as 6.17mM SDS. CMC is calculated by equating the fit lines and solving for the point of intersection. Error bars represent 1 standard deviation and are calculated from three repeat experiments per solution across an average of 10 points per repeat.

4.1. Interfacial tension measurements

The CMC for each series was determined from the intersection of the concentration-dependent section of the ST graph with the horizontal (concentration-independent) section of the graph. Below the CMC, ST is linearly dependent on the log of concentration, whereby an increase in concentration leads to a concurrent decrease in ST. Such a relationship occurs because the surfactant adsorbs to the droplet's water-air interface and creates a surfactant monolayer. Eventually, at the CMC, the interface is saturated with surfactant molecules and the minimum ST for that surfactant system is reached. Above the CMC, additional surfactant adsorption to this interface is deterred by the established adsorption layer, and surfactant molecules associate into micelles in solution, resulting in little to no further change in ST.

The CMC can be interpolated by fitting lines through the concentration-dependent and independent regions, respectively, and by then determining the intercept of the two lines. In the case of pure SDS, as shown in Fig. 7 (a), a CMC value of 7.93 mM was extracted, which is consistent with literature values of 8-8.25 mM at 298 K [70,71].

When THF was added to the SDS-CO_2 solutions, as shown in Fig. 7 (b), the measured CMC decreased by 22.2% to 6.17 mM at 298 K and atmospheric pressure. The decrease in CMC with both promoters present indicates that THF and SDS interact in solution and that this interaction causes a decrease in the amount of SDS that can adsorb to the hydrate surface. Such a significant decrease in CMC confirmed our simulation results.

4.2. HP-DSC results for CO_2 hydrate conversion

The effect of promoters (THF, SDS, and the combination of both of them) on CO_2 hydrates properties was inferred by quantities measured during our High-Pressure DSC experiments, such as the percentage of CO_2 hydrate conversion, onset temperatures, and heat released during CO_2 hydrate formation and dissociation.

Pure CO_2 hydrates were first used in our experiments to establish a baseline heat release and conversion. The pure CO_2 hydrate experiment produced a single peak with an average dissociation onset temperature of 6.29 ± 0.11 °C and heat of dissociation of 124.36 ± 1.53 J/g as produced in Figure S10 (A). This onset temperature is similar to what was obtained by Anderson [59], thereby substantiating the accuracy and validity of our experimental set-up.

Hydrate conversion was compared between CO_2 with SDS at concentrations below and above the CMC, respectively. CO_2-0.001M SDS experiments (below the CMC) produced an average dissociation onset temperature of 6.39 ± 0.11 °C, similar to the pure CO_2 system. This implies that SDS did not affect the thermodynamics of the system. As seen from Figure S10 (B), a single peak was obtained from the DSC profile, indicating a CO_2 hydrate phase with increased conversion due to the kinetic promotion. CO_2-0.038M SDS (above the CMC) experiments showed a similar DSC profile, with a single peak and an average dissociation onset temperature of 6.38 ± 0.10 °C. The hydrate conversion percentages below and above the CMC are 27 ± 1.97% and 26 ± 2.07%, respectively, with no significant difference, as shown in

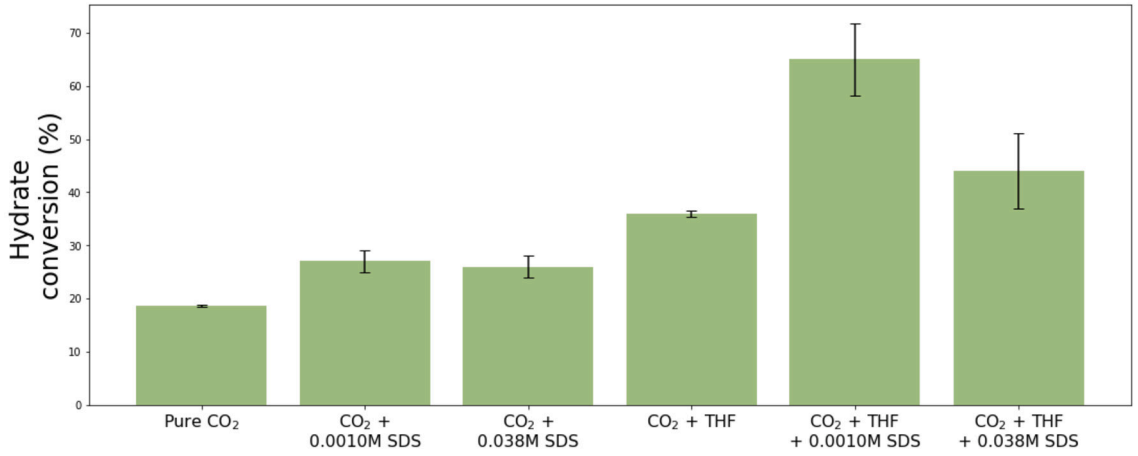

Fig. 8. Conversion determined from DSC experiments for CO_2 containing hydrate phases. The experiments were repeated in triplicates to ensure repeatability and reliability of the results.

Fig. 8. These results indicate that, with SDS alone present in the system, the presence of SDS micelles does not affect the performance of the kinetic promoter towards sI CO_2 hydrates. Such observation is consistent with the simulation results shown in Figure S9, according to which the kinetic hindrance and reduction of concentration driving force of the micelles are insignificant.

Next, 10wt% THF was added to the CO_2 hydrate system to determine the effect of THF alone. The DSC profile shown in Figure S10 (D) revealed two distinct peaks corresponding to the formation of THF hydrates and THF-CO_2 hydrates, respectively. The blue curve plotted in Figure S10 (D) is more likely to be THF hydrates as the onset temperature is 3.38 ± 0.21 °C, which is closer to that of a THF hydrate rather than a CO_2 hydrate [37]. The presence of multiple peaks suggests that the addition of THF can cause the formation of mixed hydrate phases, as shown in other works [60,72–74]. The THF-CO_2 hydrate (highlighted in orange in Figure S10 (D) has a higher dissociation onset temperature of 12.63 ± 0.82 °C as compared to CO_2 and CO_2+SDS systems shown earlier. The temperature shift conforms to the current understanding of the thermodynamic promoter role of THF. The broad peak with multiple maxima indicates that there may be CO_2-THF hydrates of different THF compositions formed and dissociated during the experiment, which aligns with previous studies [60,72]. The conversion for the THF hydrate phase was not calculated as it likely did not contain CO_2 [60,72] and thus would not factor into the total CO_2 conversion. As such, the CO_2 hydrate conversion was estimated to be 36 ± 0.61%.

THF-SDS mixtures were tested to determine the effect of the combined promoter system. At both SDS concentrations with THF present, two distinct peaks appeared, indicating hydrates of different compositions may have formed due to THF. The larger, narrow peaks (highlighted in blue) shifted well above the THF hydrate equilibrium temperature and towards the CO_2 hydrate equilibrium temperature, indicating that a pure CO_2 hydrate phase formed in place of the pure THF hydrate phase. The SDS in the system appears to have encouraged the growth of a pure sI CO_2 hydrate phase which did not exist when THF alone was present. This agrees with the conclusion drawn for methane hydrates by Kumar and colleagues [73]. In both systems, as both hydrates would contain CO_2, the conversion was estimated by adding the individual conversions for the CO_2 and CO_2-THF hydrate. At 0.001M SDS, below the CMC (Figure S10 (E)), the total conversion is 65 ± 6.76%. At 0.038M SDS above the CMC (Figure S10 (F)), the amount of CO_2 hydrate formed decreased, indicated by the lower average heat of dissociation of 83.84 ± 46.56 J/g at 5.73 ± 0.09 °C, while the CO_2-THF hydrate peak remained almost unchanged. The total CO_2 conversion in this system is computed to be 44 ± 7.09%.

The comparison of CO_2 conversion in all systems tested experimentally is presented in Fig. 8. The results first reaffirmed the discovery that a combination of THF and SDS can be synergistic. However, more importantly, while SDS added in addition to THF can increase CO_2 hydrate formation, the presence of SDS above its CMC detrimentally impacts the overall growth and conversion of the hydrate, as shown from the lower conversion. Below the CMC, the combined application of SDS and THF drastically increases conversion compared to SDS or THF alone; however, above the CMC, SDS and THF detrimentally interact, and the total conversion decreases.

5. Conclusions

5.1. Key findings

The synergism vs antagonism between THF and SDS on CO_2 hydrates was investigated using atomistic MD simulations conducted within various temperatures and system compositions. The results show that carbon dioxide hydrates grow faster with more THF at T = 269.1 K and T = 279.1 K at 25.5 bar. Increasing the temperature to 274.1 K and beyond, SDS micellar aggregates could appear, likely due to the increasing entropic driving force [65]. Lowering THF concentration can prevent the formation of SDS aggregates, which indicates that THF lowers the critical micelle concentration (CMC) of SDS. This is confirmed by results obtained from IFT experiments. Simulation results reveal that at T = 284.1 K with 100 THF molecules, the hydrates dissociated when SDS micelles existed but grew when no SDS was present at the same conditions. The HP-DSC experiments also indicate a decrease in the dissociation temperature when both THF and SDS are present.

5.2. Key improvements compared to findings in literature

The synergistic influence of THF and SDS on CO_2 hydrates has been extensively observed through various experimental investigations [15, 28]. It has been observed that the addition of an excessive amount of promoters can have a detrimental effect on their overall performance [29,75]. The present research findings shed light on the existence of an optimal surfactant concentration associated with promoting efficient hydrate growth.

5.3. Highlight of hypothesis, new concepts and innovations

The simulation and experiment results indicate that the SDS aggregates behave like thermodynamic inhibitors as they trap THF molecules, essentially removing them and the SDS themselves from the hydrate-liquid interface. Removing THF reduces its thermodynamic stabilisation ability. This phenomenon explains the presence of optimal surfactant

concentration related to promoting hydrate growth. CO_2 conversion results obtained from DSC experiments also reinforced this hypothesis. In addition to being consistent with the simulation results, the experiments also show that the CO_2 uptake in hydrates strongly depends on the synergism among the two promoters, with the best results obtained here showing 21% to 46% increase in CO_2 uptake compared to systems without promoters, as well as with system with a sub-optimal composition of the promoters cocktail.

5.4. *Vision for future work*

These results provide insights into understanding the microscopic behaviours of promoters on hydrate growth and how promoters can interact synergistically and/or antagonistically depending on their relative concentrations and the system conditions. Because our results show the possibility of SDS forming aggregates at very low concentrations, future research should aim at uncovering the molecular mechanisms by which SDS acts as a kinetic promoter at low concentrations, below the CMC.

CRediT authorship contribution statement

AS planned the project. XC performed the simulations. MS and AP helped with algorithm development and validation. CK planned the experimental validation. JW conducted the experiments. XC and JW prepared the first draft of the manuscript. All Authors edited the manuscript. AS and CK obtained financial support and managed the project.

Declaration of competing interest

The Authors declare no conflict of interest.

Data availability

Data will be made available on request.

Acknowledgements

Xinrui Cai would like to express her gratitude towards the A&BK studentship that sponsored this project. Alberto Striolo is grateful to the Asahi Chair in Chemical Engineering at the University of Oklahoma, as well as to the EPSRC grant number EP/T004282/1 for financial support. Matteo Salvalaglio acknowledges funding from the Crystallization in the Real World EPSRC Programme Grant (Grant EP/R018820/1) and the EPSRC Frontier Guarantee Grant (EP/X033139/1). Joshua Worley and Carolyn Koh acknowledge funding from the NSF under the CBET grant 2015201 for experimental work. The authors gratefully acknowledge the Archer2 and UCL Myriad teams for providing access to their supercomputing facilities and technical support, which have greatly advanced this research project.

Appendix A. Supplementary material

Supplementary material related to this article can be found online at https://doi.org/10.1016/j.jcis.2023.11.136.

References

[1] B.A. Buffett, Clathrate hydrates, Annu. Rev. Earth Planet. Sci. 28 (may 2000) 477–507.
[2] E.D. Sloan Jr., C.A. Koh, Clathrate Hydrates of Natural Gases, 3rd ed., CRC Press, sep 2007.
[3] E.D. Sloan, Fundamental principles and applications of natural gas hydrates, Nature 426 (6964) (2003) 353–359.
[4] H.P. Veluswamy, P. Linga, Macroscopic kinetics of hydrate formation of mixed hydrates of hydrogen/tetrahydrofuran for hydrogen storage, Int. J. Hydrog. Energy 38 (apr 2013) 4587–4596.
[5] H.J. Lee, J.D. Lee, P. Linga, P. Englezos, Y.S. Kim, M.S. Lee, Y.D. Kim, Gas hydrate formation process for pre-combustion capture of carbon dioxide, Energy 35 (6) (2010) 2729–2733.
[6] M. Yang, H. Zhou, P. Wang, N. Li, Y. Song, Hydrate-based CO2 capture from flue gas in constant pressure process with the presence of THF, Energy Proc. 142 (2017) 3939–3943.
[7] S. Lee, L. Liang, D. Riestenberg, O.R. West, C. Tsouris, E. Adams, CO2 hydrate composite for ocean carbon sequestration, Environ. Sci. Technol. 37 (aug 2003) 3701–3708.
[8] T. Saikia, A. Sultan, Hydrate-based CO2 separation, in: Emerging Carbon Capture Technologies, Elsevier Inc., 2022, pp. 193–237, ch. 7.
[9] P.W. Wang, D.T. Wu, S.T. Lin, Promotion mechanism for the growth of CO2 hydrate with urea using molecular dynamics simulations, Chem. Commun. 57 (43) (2021) 5330–5333.
[10] H. Dashti, L. Zhehao Yew, X. Lou, Recent advances in gas hydrate-based CO2 capture, J. Nat. Gas Sci. Eng. 23 (2015) 195–207.
[11] H. Hoteit, M. Fahs, M.R. Soltanian, Assessment of CO2 injectivity during sequestration in depleted gas reservoirs, Geosciences 9 (may 2019) 199.
[12] J.-H. Sa, B.R. Lee, D.-H. Park, K. Han, H.D. Chun, K.-H. Lee, Amino acids as natural inhibitors for hydrate formation in CO2 sequestration, Environ. Sci. Technol. 45 (jul 2011) 5885–5891.
[13] A.A. Majid, J. Worley, C.A. Koh, Thermodynamic and kinetic promoters for gas hydrate technological applications, Energy Fuels 35 (23) (2021) 19288–19301.
[14] Y. Li, A.M. Gambelli, F. Rossi, S. Mei, Effect of promoters on CO2 hydrate formation: thermodynamic assessment and microscale Raman spectroscopy/hydrate crystal morphology characterization analysis, Fluid Phase Equilib. 550 (2021) 113218.
[15] H.P. Veluswamy, K.P. Premasinghe, P. Linga, CO2 hydrates - effect of additives and operating conditions on the morphology and hydrate growth, Energy Proc. 105 (2017) 5048–5054.
[16] N. Xu, Y. Liu, Z. Cheng, S. Wang, L. Jiang, Y. Song, Morphology-based kinetic study of the formation of carbon dioxide hydrates with promoters, Energy Fuels 34 (jun 2020) 7307–7315.
[17] O. Salako, C. Lo, J. Zhang, A. Couzis, P. Somasundaran, J. Lee, Adsorption of sodium dodecyl sulfate onto clathrate hydrates in the presence of salt, J. Colloid Interface Sci. 386 (nov 2012) 333–337.
[18] J.S. Zhang, S. Lee, J.W. Lee, Kinetics of methane hydrate formation from SDS solution, Ind. Eng. Chem. Res. 46 (sep 2007) 6353–6359.
[19] A. Kumar, G. Bhattacharjee, B.D. Kulkarni, R. Kumar, Role of surfactants in promoting gas hydrate formation, Ind. Eng. Chem. Res. 54 (dec 2015) 12217–12232.
[20] J. Yoslim, P. Linga, P. Englezos, Enhanced growth of methane–propane clathrate hydrate crystals with sodium dodecyl sulfate, sodium tetradecyl sulfate, and sodium hexadecyl sulfate surfactants, J. Cryst. Growth 313 (dec 2010) 68–80.
[21] C. Lo, J. Zhang, P. Somasundaran, J.W. Lee, Investigations of surfactant effects on gas hydrate formation via infrared spectroscopy, J. Colloid Interface Sci. 376 (jun 2012) 173–176.
[22] H. Liang, D. Guan, Y. Liu, L. Zhang, J. Zhao, L. Yang, Y. Song, Kinetic process of upward gas hydrate growth and water migration on the solid surface, J. Colloid Interface Sci. 626 (nov 2022) 1003–1014.
[23] S.P. Kang, H. Lee, C.S. Lee, W.M. Sung, Hydrate phase equilibria of the guest mixtures containing CO2, N2 and tetrahydrofuran, Fluid Phase Equilib. 185 (1–2) (2001) 101–109.
[24] A. Phan, H. Schlösser, A. Striolo, Molecular mechanisms by which tetrahydrofuran affects CO2 hydrate growth: implications for carbon storage, Chem. Eng. J. 418 (o) (December 2020) 34–37, 2021.
[25] L. Liu, Y. Yao, X. Zhou, Y. Zhang, D. Liang, Improved formation kinetics of carbon dioxide hydrate in brine induced by sodium dodecyl sulfate, Energies 14 (8) (2021).
[26] D.L. Zhong, S.Y. He, D.J. Sun, C. Yang, Comparison of methane hydrate formation in stirred reactor and porous media in the presence of SDS, Energy Proc. 61 (2014) 1573–1576.
[27] N.S. Molokitina, A.N. Nesterov, L.S. Podenko, A.M. Reshetnikov, Carbon dioxide hydrate formation with SDS: further insights into mechanism of gas hydrate growth in the presence of surfactant, Fuel 235 (o) (March 2018) 1400–1411, 2019.
[28] J.P. Torré, M. Ricaurte, C. Dicharry, D. Broseta, CO2 enclathration in the presence of water-soluble hydrate promoters: hydrate phase equilibria and kinetic studies in quiescent conditions, Chem. Eng. Sci. 82 (2012) 1–13.
[29] H. Wang, Q. Wu, B. Zhang, Influence of THF and THF/SDS on the kinetics of CO2 hydrate formation under stirring, Front. Energy Res. 9 (feb 2021).
[30] J.S. Zhang, C. Lo, P. Somasundaran, J.W. Lee, Competitive adsorption between SDS and carbonate on tetrahydrofuran hydrates, J. Colloid Interface Sci. 341 (jan 2010) 286–288.
[31] J. Tang, D. Zeng, C. Wang, Y. Chen, L. He, N. Cai, Study on the influence of SDS and THF on hydrate-based gas separation performance, Chem. Eng. Res. Des. 91 (sep 2013) 1777–1782.
[32] X. Lv, D. Lu, Y. Liu, S. Zhou, J. Zuo, H. Jin, B. Shi, E. Li, Study on methane hydrate formation in gas-water systems with a new compound promoter, RSC Adv. 9 (57) (2019) 33506–33518.
[33] A. Demurov, R. Radhakrishnan, B.L. Trout, Computations of diffusivities in ice and CO2 clathrate hydrates via molecular dynamics and Monte Carlo simulations, J. Chem. Phys. 116 (jan 2002) 702–709.

[34] N.I. Papadimitriou, I.N. Tsimpanogiannis, I.G. Economou, A.K. Stubos, Monte Carlo simulations of the separation of a binary gas mixture (CH4 + CO2) using hydrates, Phys. Chem. Chem. Phys. 20 (44) (2018) 28026–28038.
[35] Y.J. Lee, T. Kawamura, Y. Yamamoto, J.H. Yoon, Phase equilibrium studies of tetrahydrofuran (THF) + CH4, THF + CO2, CH4 + CO2, and THF + CO2 + CH4 hydrates, J. Chem. Eng. Data 57 (12) (2012) 3543–3548.
[36] F. Takeuchi, M. Hiratsuka, R. Ohmura, S. Alavi, A.K. Sum, K. Yasuoka, Water proton configurations in structures I, II, and H clathrate hydrate unit cells, J. Chem. Phys. 138 (12) (2013).
[37] A. Delahaye, L. Fournaison, S. Marinhas, I. Chatti, J.-P. Petitet, D. Dalmazzone, W. Fürst, Effect of THF on equilibrium pressure and dissociation enthalpy of CO2 hydrates applied to secondary refrigeration, Ind. Eng. Chem. Res. 45 (jan 2006) 391–397.
[38] L. Jensen, K. Thomsen, N. von Solms, S. Wierzchowski, M.R. Walsh, C.A. Koh, E.D. Sloan, D.T. Wu, A.K. Sum, Calculation of liquid water-hydrate-methane vapor phase equilibria from molecular simulations, J. Phys. Chem. B 114 (may 2010) 5775–5782.
[39] J.M. Míguez, M.M. Conde, J.P. Torré, F.J. Blas, M.M. Piñeiro, C. Vega, Molecular dynamics simulation of CO2 hydrates: prediction of three phase coexistence line, J. Chem. Phys. 142 (12) (2015).
[40] M.M. Conde, C. Vega, Determining the three-phase coexistence line in methane hydrates using computer simulations, J. Chem. Phys. 133 (aug 2010) 064507.
[41] J.G. Harris, K.H. Yung, Carbon dioxide's liquid-vapor coexistence curve and critical properties as predicted by a simple molecular model, J. Phys. Chem. 99 (aug 1995) 12021–12024.
[42] Y.T. Tung, L.J. Chen, Y.P. Chen, S.T. Lin, Growth of structure I carbon dioxide hydrate from molecular dynamics simulations, J. Phys. Chem. C 115 (15) (2011) 7504–7515.
[43] P. Procacci, PrimaDORAC: a free web interface for the assignment of partial charges, chemical topology, and bonded parameters in organic or drug molecules, J. Chem. Inf. Model. 57 (jun 2017) 1240–1245.
[44] H. Dominguez, M.L. Berkowitz, Computer simulations of sodium dodecyl sulfate at liquid/liquid and liquid/vapor interfaces, J. Phys. Chem. B 104 (jun 2000) 5302–5308.
[45] V.K. Michalis, I.N. Tsimpanogiannis, A.K. Stubos, I.G. Economou, Direct phase coexistence molecular dynamics study of the phase equilibria of the ternary methane-carbon dioxide-water hydrate system, Phys. Chem. Chem. Phys. 18 (34) (2016) 23538–23548.
[46] H. Berendsen, D. van der Spoel, R. van Drunen, GROMACS: a message-passing parallel molecular dynamics implementation, Comput. Phys. Commun. 91 (sep 1995) 43–56.
[47] H.J.C. Berendsen, J.P.M. Postma, W.F. van Gunsteren, A. DiNola, J.R. Haak, Molecular dynamics with coupling to an external bath, J. Chem. Phys. 81 (oct 1984) 3684–3690.
[48] D.J. Evans, B.L. Holian, The Nose–Hoover thermostat, J. Chem. Phys. 83 (oct 1985) 4069–4074.
[49] M. Parrinello, A. Rahman, Crystal structure and pair potentials: a molecular-dynamics study, Phys. Rev. Lett. 45 (oct 1980) 1196–1199.
[50] T. Yagasaki, M. Matsumoto, H. Tanaka, Mechanism of slow crystal growth of tetrahydrofuran clathrate hydrate, J. Phys. Chem. C 120 (feb 2016) 3305–3313.
[51] Y. Zhang, S.E. Feller, B.R. Brooks, R.W. Pastor, Computer simulation of liquid/liquid interfaces. I. Theory and application to octane/water, J. Chem. Phys. 103 (dec 1995) 10252–10266.
[52] S. Adisasmito, R.J. Frank, E.D. Sloan, Hydrates of carbon dioxide and methane mixtures, J. Chem. Eng. Data 36 (jan 1991) 68–71.
[53] P. Rodger, T. Forester, W. Smith, Simulations of the methane hydrate/methane gas interface near hydrate forming conditions conditions, Fluid Phase Equilib. 116 (mar 1996) 326–332.
[54] T. Bui, F. Sicard, D. Monteiro, Q. Lan, M. Ceglio, C. Burress, A. Striolo, Antiagglomerants affect gas hydrate growth, J. Phys. Chem. Lett. 9 (12) (2018) 3491–3496.
[55] K.W. Hall, S. Carpendale, P.G. Kusalik, Evidence from mixed hydrate nucleation for a funnel model of crystallization, 2016.
[56] G.A. Tribello, F. Giberti, G.C. Sosso, M. Salvalaglio, M. Parrinello, Analyzing and driving cluster formation in atomistic simulations, J. Chem. Theory Comput. 13 (3) (2017) 1317–1327.
[57] L. Kollias, R. Rousseau, V.-A. Glezakou, M. Salvalaglio, Understanding metal–organic framework nucleation from a solution with evolving graphs, J. Am. Chem. Soc. 144 (25) (2022) 11099–11109.
[58] S. Denning, A.A. Majid, J.M. Lucero, J.M. Crawford, M.A. Carreon, C.A. Koh, Metal–organic framework HKUST-1 promotes methane hydrate formation for improved gas storage capacity, ACS Appl. Mater. Interfaces 12 (nov 2020) 53510–53518.
[59] G.K. Anderson, Enthalpy of dissociation and hydration number of carbon dioxide hydrate from the Clapeyron equation, J. Chem. Thermodyn. 35 (jul 2003) 1171–1183.
[60] M.C. Martínez, D. Dalmazzone, W. Fürst, A. Delahaye, L. Fournaison, Thermodynamic properties of THF + CO2 hydrates in relation with refrigeration applications, AIChE J. 54 (apr 2008) 1088–1095.
[61] Q. Sun, Y.T. Kang, Review on CO2 hydrate formation/dissociation and its cold energy application, Renew. Sustain. Energy Rev. 62 (2016) 478–494.
[62] P. Zhang, Q. Wu, C. Mu, X. Chen, Nucleation mechanisms of CO2 hydrate reflected by gas solubility, Sci. Rep. 8 (1) (2018) 1–12.
[63] L.S. Chu, D.T. Wu, S.T. Lin, Theory and kinetic Monte Carlo simulation of guest molecule transport in sI clathrate hydrates based on cage hopping, J. Phys. Chem. C 123 (17) (2019) 11233–11243.
[64] M.D. Smith, B. Mostofian, L. Petridis, X. Cheng, J.C. Smith, Molecular driving forces behind the tetrahydrofuran-water miscibility gap, J. Phys. Chem. B 120 (4) (2016) 740–747.
[65] L. Maibaum, A.R. Dinner, D. Chandler, Micelle formation and the hydrophobic effect, J. Phys. Chem. B 108 (may 2004) 6778–6781.
[66] M. Manabe, M. Koda, The effect of poly(oxyethylene) alkyl ethers, alkanediols, and alkanols on the critical micelle concentration of sodium dodecyl sulfate, Bull. Chem. Soc. Jpn. 51 (6) (1978) 1599–1601.
[67] N. Riesco, J. Trusler, Novel optical flow cell for measurements of fluid phase behaviour, Fluid Phase Equilib. 228–229 (feb 2005) 233–238.
[68] A. Phan, M. Stamatakis, C.A. Koh, A. Striolo, Microscopic insights on clathrate hydrate growth from non-equilibrium molecular dynamics simulations, J. Colloid Interface Sci. 649 (nov 2023) 185–193.
[69] T. Daimaru, A. Yamasaki, Y. Yanagisawa, Effect of surfactant carbon chain length on hydrate formation kinetics, J. Pet. Sci. Eng. 56 (mar 2007) 89–96.
[70] T.P. Niraula, A. Bhattarai, S.K. Chatterjee, Critical micelle concentration of sodium dodecyl sulphate in pure water and in methanol-water mixed solvent media in presence and absence of KCl by surface tension and viscosity methods, BIBECHANA 11 (may 2014) 103–112.
[71] Y. Moroi, K. Motomura, R. Matuura, The critical micelle concentration of sodium dodecyl sulfate-bivalent metal dodecyl sulfate mixtures in aqueous solutions, J. Colloid Interface Sci. 46 (jan 1974) 111–117.
[72] Q. Sun, S. Kim, Y.T. Kang, Study on dissociation characteristics of CO2 hydrate with THF for cooling application, Appl. Energy 190 (mar 2017) 249–256.
[73] A. Kumar, R. Kumar, P. Linga, Sodium dodecyl sulfate preferentially promotes enclathration of methane in mixed methane-tetrahydrofuran hydrates, iScience 14 (apr 2019) 136–146.
[74] A. Kumar, N. Daraboina, R. Kumar, P. Linga, Experimental investigation to elucidate why tetrahydrofuran rapidly promotes methane hydrate formation kinetics: applicable to energy storage, J. Phys. Chem. C 120 (dec 2016) 29062–29068.
[75] D. Mech, P. Gupta, J.S. Sangwai, Kinetics of methane hydrate formation in an aqueous solution of thermodynamic promoters (THF and TBAB) with and without kinetic promoter (SDS), J. Nat. Gas Sci. Eng. 35 (sep 2016) 1519–1534.